

Frequency-Independent RC Circuit Model for One-Dimensional Carbon Nanostructures

Francisco R. Madriz, Toshishige Yamada, *Member, IEEE*, Xuhui Sun, *Member, IEEE*,
Josh G. Nickel, and Cary Y. Yang, *Fellow, IEEE*

Abstract—We demonstrate that a frequency-independent parallel RC circuit is the simplest model that accurately describes high-frequency electrical conduction in 1-D nanostructures. The resistance is determined from dc measurement, and the capacitance is extracted directly from the measured S -parameters for a ground–signal–ground test structure, without using any fitting parameter. The methodology is applied to carbon nanofibers, and the RC model yields results that are within ± 0.5 dB and $\pm 5^\circ$ of the measured S -parameters up to 50 GHz. The model is further justified by examining the relationship between S - and Y -parameters of the test network.

Index Terms—Carbon nanofibers (CNFs), frequency-independent RC circuit model, S -parameters.

I. INTRODUCTION

THE STUDY of carbon-based nanostructures as a potential interconnect material for next-generation integrated circuit technology has drawn increasing interest in recent years [1]–[4]. Electron transport at dc in carbon nanotubes and carbon nanofibers (CNFs) has been investigated at length [5], [6]. In order to predict the behavior of 1-D nanostructures in a circuit operating at high frequencies, a lumped parameter model is necessary for implementation in an industry-standard circuit simulator. To this end, three different models have been proposed. The first one treats low-resistance (a few ohms) nanostructures as a transmission line modeled with an RLC network [7]. Most nanostructures have much larger total resistance. The second one models the nanostructure–electrode contact with a parallel RC and the “bulk” with an RLC network [8]. The third model [9] omits the parallel capacitor in [8]. The models in [8] and [9] are reasonable circuit representations of nanostructures in contact with two electrodes, but the number of frequency-dependent parameters is prohibitively high for implementation in a circuit simulator.

Manuscript received November 22, 2009. First published February 25, 2010; current version published March 24, 2010. This work was supported by the U.S. Army Space and Missile Defense Command SMDC and carries distribution Statement A, approved for public release, distribution unlimited. The review of this letter was arranged by Editor L. Selmi.

F. R. Madriz, T. Yamada, and C. Y. Yang are with the Center for Nanostructures, Santa Clara University, Santa Clara, CA 95053 USA (e-mail: fmadriz@scu.edu; tyamada@scu.edu; cyang@scu.edu).

X. Sun is with the Center for Nanostructures, Santa Clara University, Santa Clara, CA 95053 USA, and also with the Functional Nano and Soft Materials Laboratory and the Jiangsu Key Laboratory for Carbon-Based Functional Materials and Devices, Soochow University, Suzhou 215123, China (e-mail: sunxuhui@gmail.com).

J. G. Nickel is with the Department of Electrical Engineering, Santa Clara University, Santa Clara, CA 95053 USA (e-mail: jnickel@scu.edu).

Color versions of one or more of the figures in this letter are available online at <http://ieeexplore.ieee.org>.

Digital Object Identifier 10.1109/LED.2010.2040023

Recently, we have demonstrated that the measured S -parameters of ten CNF test devices can be accurately reproduced using a frequency-independent parallel $R_F C_F$ circuit model up to 50 GHz [10]. Transport within the CNF is ohmic, and kinetic inductance is not present [11], [12]. The magnetic inductance for a metal–oxide–substrate system is given by $L_m \approx (\mu/2\pi) \ln(4h/d)$ [12], where μ is the permeability and h and d are the oxide thickness and the metal cylinder diameter, respectively. In our experiment, h is 3 μm . For CNFs whose diameters d are between 70 and 200 nm, their respective magnetic inductance value is < 1 pH/ μm . Thus, L_m is negligible below 1 THz.

In this letter, we introduce a methodology in which a simple frequency-independent parallel RC circuit extracted directly from measurements is sufficient to describe high-frequency electrical conduction in nanostructures [10]. Unlike our previous work [10], no fitting parameter is employed. Twenty CNFs with two different types of CNF–electrode contacts are measured, with diameters ranging from 70 to 200 nm.

II. EXPERIMENT

The fabrication procedure was described in detail elsewhere [1], [10]. In five of the 20 devices, platinum was deposited onto the drop-casted electrode contacts using focused ion beam to obtain improved contacts. The dc resistance R_{dc} between the signal pads is then measured for each of the 20 devices. R_{dc} consists of probe contact resistance R_T , signal pad resistance, CNF bulk resistance, and contact resistance between CNF and electrodes R_C . The two-port S -parameters of the test structure with and without CNF are measured from 0.1 to 50 GHz using a vector network analyzer (VNA). Note that several open test structures in close proximity to the one with CNF are used in the de-embedding process, giving rise to errors due to process variations, to be addressed in Section IV.

III. CIRCUIT MODEL PARAMETER EXTRACTION

We de-embed the test structure upon which the nanostructure is placed using an equivalent circuit for the fabricated ground–signal–ground configuration, as shown in Fig. 1. The shaded components constitute the open test structure, or the “open circuit” (OC) before the nanostructure is placed between the two signal pads. The equivalent circuit model of the nanostructure in its admittance form is given in the inset in Fig. 1. Using this model, $G_F(\omega)$ and $C_F(\omega)$ of the CNF (including contacts) are extracted directly from the simple relation $y(\omega) = G_F(\omega) + j\omega C_F(\omega) = Y_{21}^{\text{OC}}(\omega) - Y_{21}^{\text{CNF}}(\omega)$. Y_{21}^{CNF} is

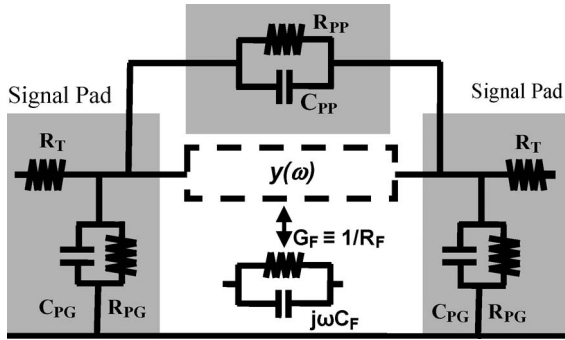


Fig. 1. Circuit model of the test network [10]. The shaded components represent the signal pads and coupling between input and output, with CNF connecting the open gap. At a given frequency, both S_{11} and S_{21} are measured. CNF and its contacts are represented in its admittance form $y(\omega)$. At low frequencies, $C_{PP} = 1.1$ fF, $C_{PG} = 50$ fF, $R_{PP} = 1$ M Ω , and $R_{PG} = 30$ k Ω .

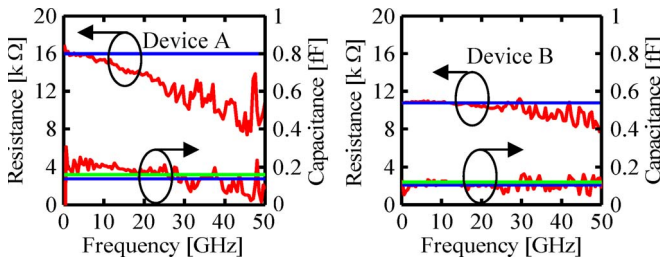


Fig. 2. (Red lines) Extracted $R_F(\omega)$ and $C_F(\omega)$ from S -parameters are shown for devices A (drop-casted contacts) and B (Pt-deposited contacts). (Blue line) R_{dc} is the measured dc resistance, and (blue line) C_{Fav} is the average value of $C_F(\omega)$. (Green line) C_{Ffit} from fitting is also shown for comparison.

obtained from the measured S_{21} of the test structure with CNF present, and Y_{21}^{OC} is computed using the equivalent circuit from the open structure.

While both G_F and C_F are frequency dependent in general and can be extracted directly using $y(\omega)$, one can exploit the fact that $G_F(0) = 1/R_{dc}$ and use a *frequency-independent RC* circuit to represent the CNF and its contacts. The constant capacitance can be a fitting parameter as we reported in [10], or more systematically and without loss of accuracy as we show here, it is computed as the average of the extracted $C_F(\omega)$ over the measurement frequency range C_{Fav} .

IV. RESULTS AND DISCUSSION

Results for two representative devices, one for each type of electrode contacts, are shown in Fig. 2. R_{dc} and the extracted $R_F(\omega)$ for both devices are shown together with $C_F(\omega)$, C_{Fav} , and C_{Ffit} obtained from fitting. $R_F(\omega)$ for drop-casted device A shows a strong dependence on frequency, decreasing from 16 k Ω at dc to 9 k Ω at 50 GHz, while $C_F(\omega)$ decreases from 0.3 to 0.1 fF. On the other hand, for device B with Pt deposited onto the drop-casted electrode contacts, $R_F(\omega)$ shows a much weaker dependence on frequency as it decreases from 10.8 to 8.5 k Ω , while $C_F(\omega)$ remains fairly constant over the entire frequency range. This weak ω dependence in device B indicates that the nanofiber resistance is fairly constant in this frequency range and that the contact impedance, while not completely eliminated, is reduced significantly.

In the constant *RC* model, the resistance is set to R_{dc} , which is experimentally determined from dc measurement and

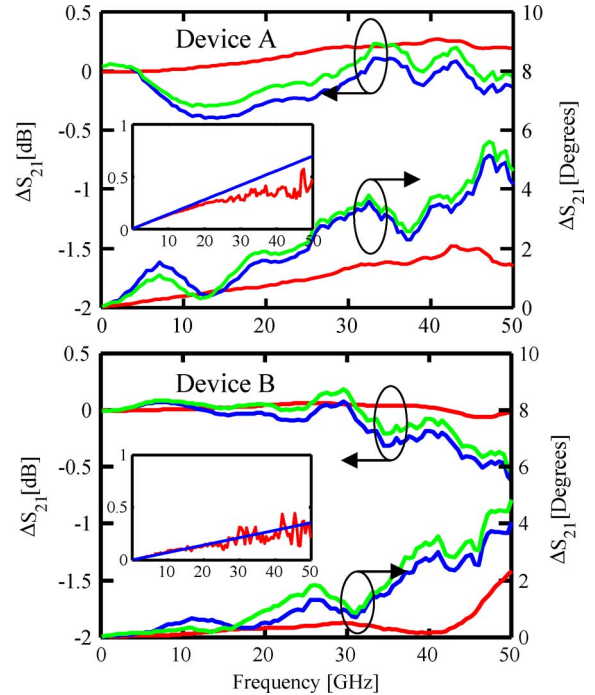


Fig. 3. S_{21} magnitude (in decibels) and phase comparison between measurement and model for devices A and B: Errors for $R_F(\omega)$ and $C_F(\omega)$ in red, for R_{dc} and C_{Fav} in blue, and for R_{dc} and C_{Ffit} in green. The inset for either device shows (red line) $\omega R_F(\omega)C_F(\omega)$ and (blue line) $\omega R_{dc}C_{Fav}$ versus frequency in gigahertz.

includes the CNF bulk resistance R_{CNF} and the contact resistance with each electrode R_C [8]. Thus, $R_{dc} = R_F(0) = 2R_C(0) + R_{CNF}(0)$. The capacitance is assumed to be the average of the extracted $C_F(\omega)$ over the measured frequency range, or C_{Fav} . Contact resistance R_C is generally frequency independent, and if the contact capacitance is small, using R_{dc} to replace $R_F(\omega)$ over the measured frequency range is a reasonable representation of the resistive behavior of the entire device. Furthermore, since the CNF capacitance is very small because of its size, the resulting impedance is dominated by its resistive component, and it is a good approximation to assume an average value for C_F . These assumptions are verified by the results for either device, as shown in Fig. 2. This finding suggests that the capacitance in the constant *RC* model serves largely as a correction to a pure resistive model for devices with significant contact impedance.

Fig. 3 shows the corresponding magnitude (in decibels) and phase differences between the measured and modeled S_{21} for both devices. The red lines represent the errors when using the frequency-dependent elements $R_F(\omega)$ and $C_F(\omega)$, which are nonzero due to process variations between the open test structure and the test structure with the nanofiber in place. The errors introduced by using R_{dc} and C_{Fav} are shown in blue in Fig. 3. Note that the error for $|S_{21}|$ is ± 0.5 dB, and for the phase, it is $< 5^\circ$ for either device. For comparison, the errors for $|S_{21}|$ using the fitted constant value C_{Ffit} are also shown. No significant difference between the results from using either constant capacitance is observed.

To examine the constant *RC* model further and to validate its utility, we proceed to derive the S -parameters of the test

network with and without the nanostructure as a function of the admittance matrix. The VNA load admittance is given by $Y_0 = 0.02$ S, the electrode-ground admittance by $Y_{PG}(\omega) = 1/R_{PG}(\omega) + j\omega C_{PG}(\omega)$, the electrode-electrode admittance by $Y_{PP}(\omega) = 1/R_{PP}(\omega) + j\omega C_{PP}(\omega)$, and the CNF admittance by $y = G_F + j\omega C_F$. R_T ($\sim 2 \Omega$) can be neglected [10]. From their extracted values, we observe that $|Y_0| \gg |y| \sim |Y_{PG}| \gg |Y_{PP}|$ over the entire frequency range. Thus, we deduce the following.

- 1) Reflections without and with a CNF, S_{11}^{OC} and S_{11}^{CNF} , are both approximated by $1 - [Y_{PG}(\omega)/Y_0]^2$. The dependence is predominantly on Y_{PG} over the entire frequency range and not on the admittance of the CNF, and the reflection is nearly unity as expected.
- 2) Transmission without a nanostructure S_{21}^{CNF} , is approximated by $2Y_{PP}(\omega)/Y_0$. As expected, S_{21}^{OC} is dependent on $Y_{PP}(\omega)$.
- 3) Transmission with nanostructure present, S_{21}^{CNF} , is approximated by $2[y + Y_{PP}(\omega)]/Y_0$ for frequency $< \sim 10$ GHz. This expression is further reduced to $2y/Y_0$ since $|y| \gg |Y_{PP}|$. The measured monotonic increase in $|S_{21}^{CNF}|$ and $\arg(S_{21}^{CNF})$ for $\omega < 10$ GHz is consistent with this simplified expression and reproduced using the constant RC model [10]. Above 10 GHz, y is comparable with Y_{PG} or Y_{PP} , and the approximation is no longer valid, resulting in a more complex behavior which is also predicted using the constant RC model.

From the insets in Fig. 3, the relation $\omega R_F(\omega)C_F(\omega) < 1$ is valid for the entire frequency range, and thus, $1/R_F$ is dominant in y . By replacing $R_F(\omega)$ and $C_F(\omega)$ with constants R_{dc} and C_{Fav} in the model proposed here, the result (blue line) approximates its ω -dependent counterpart (red line) quite well while keeping $1/R_F$ dominant in y as long as $\omega R_{dc}C_{Fav} < 1$. The validity of the constant RC model depends on the difference between the blue and red lines or whether the relation $\omega R_F(\omega)C_F(\omega) \sim \omega R_{dc}C_{Fav}$ holds true. Comparing the insets in Fig. 3, we observe that, for device B, the blue $\omega R_{dc}C_{Fav}$ line approximates the red $\omega R_F(\omega)C_F(\omega)$ behavior very well over the entire frequency range, supporting the constant RC model. For device A, the two lines in the inset coincide for frequencies below 10 GHz and diverge at higher frequencies. Nevertheless, as shown in Fig. 3, the frequency-independent RC model reproduces the measured S_{21} very well over the entire frequency range for either device. This finding further supports our earlier suggestion that, for a nanostructure with good contacts such as device B with low contact impedance, its

behavior up to a very high frequency can be simply represented by its dc resistance.

V. CONCLUSION

We have developed and validated an analytical approach to extract a frequency-independent parallel RC circuit model for nanostructures, directly from measurements with no fitting parameters. The CNF, in this case, behaves mostly like a resistor up to 50 GHz, with its resistance being the total dc resistance from the bulk and contacts with electrodes. The capacitance in the model represents a correction that takes into account the contact impedance. The difference between the model and experiment comes primarily from process variations. The model is further justified by considering the relation between the S - and Y -parameters in the test network.

REFERENCES

- [1] Q. Ngo, T. Yamada, M. Suzuki, Y. Ominami, A. M. Cassell, J. Li, M. Meyyappan, and C. Y. Yang, "Structural and electrical characterization of carbon nanofibers for interconnect via applications," *IEEE Trans. Nanotechnol.*, vol. 6, no. 6, pp. 688–695, Nov. 2007.
- [2] K.-H. Koo, H. Cho, P. Kapur, and K. C. Saraswat, "Performance comparison between carbon nanotubes, optical, and Cu for future high-performance on-chip interconnect applications," *IEEE Trans. Electron Devices*, vol. 54, no. 12, pp. 3206–3215, Dec. 2007.
- [3] H. Li, C. Xu, N. Srisvastava, and K. Banerjee, "Carbon nanomaterials for next-generation interconnects and passives: Physics, status, and prospect," *IEEE Trans. Electron Devices*, vol. 56, no. 9, pp. 1799–1821, Sep. 2009.
- [4] International Technology Roadmap of Semiconductor, 2007 edition. [Online]. Available: <http://www.itrs.net/Links/2007ITRS/Home2007.htm>
- [5] M. S. Dresselhaus, G. Dresselhaus, and P. Avouris, Eds., *Topics in Applied Physics, Carbon Nanotubes: Synthesis, Structure, Properties and Applications*. New York: Springer-Verlag, 2000.
- [6] T. Yamada, T. Saito, D. Fabris, and C. Y. Yang, "Electrothermal analysis of breakdown in carbon nanofiber interconnects," *IEEE Electron Device Lett.*, vol. 30, no. 5, pp. 469–471, May 2009.
- [7] P. J. Burke, "An RF circuit model for carbon nanotubes," *IEEE Trans. Nanotechnol.*, vol. 2, no. 1, pp. 55–58, Mar. 2003.
- [8] S. C. Jun, X. M. H. Huang, S. Moon, H. J. Kim, J. Hone, Y. W. Jin, and J. M. Kim, "Passive electrical properties of multi-walled carbon nanotubes up to 0.1 THz," *New J. Phys.*, vol. 9, p. 265, Aug. 2007.
- [9] J. J. Plombon, K. P. O'Brien, F. Gstrein, and V. M. Dubin, "High-frequency electrical properties of individual and bundled carbon nanotubes," *Appl. Phys. Lett.*, vol. 90, no. 6, p. 063 106, Feb. 2007.
- [10] F. R. Madriz, J. R. Jameson, S. Krishnan, X. Sun, and C. Y. Yang, "Circuit modeling of high-frequency conduction in carbon nanofibers," *IEEE Trans. Electron Devices*, vol. 56, no. 8, pp. 1557–1561, Aug. 2009.
- [11] S. Frank, P. Poncharal, Z. L. Wang, and W. A. de Heer, "Carbon nano tube quantum resistor," *Science*, vol. 280, no. 5370, pp. 1744–1746, Jun. 1998.
- [12] T. Yamada, F. R. Madriz, and C. Y. Yang, "Inductance in one-dimensional nanostructures," *IEEE Trans. Electron Devices*, vol. 56, no. 9, pp. 1834–1839, Sep. 2009.